

Self-similar pressure oscillations in neutron star envelopes as probes of neutron star structure

A. I. Chugunov*

Ioffe Physicotechnical Institute, St. Petersburg, Russia

27 November 2018

ABSTRACT

We study eigenmodes of acoustic oscillations of high multipolarity $l \sim 100 - 1000$ and high frequency (~ 100 kHz), localized in neutron star envelopes. We show that the oscillation problem is self-similar. Once the oscillation spectrum is calculated for a given equation of state (EOS) in the envelope and given stellar mass M and radius R , it can be rescaled to a star with any M and R (but the same EOS in the envelope). For $l \gtrsim 300$ the modes can be subdivided into the outer and inner ones. The outer modes are mainly localized in the outer envelope. The inner modes are mostly localized near the neutron drip point, being associated with the softening of the EOS after the neutron drip. We calculate oscillation spectra for the EOSs of cold-catalyzed and accreted matter and show that the spectra of the inner modes are essentially different. A detection and identification of high-frequency pressure modes would allow one to infer M and R and determine also the EOS in the envelope (accreted or ground-state) providing thus a new and simple method to explore the main parameters and internal structure of neutron stars.

Key words: stars: neutron – stars: oscillations.

1 INTRODUCTION

Neutron stars can be considered as resonators where various oscillation modes can be excited. These oscillations are attracting much attention because, in principle, they can be used to study the internal structure of neutron stars. Some of them (for instance, r-modes) can be accompanied by gravitational radiation. Because neutron stars are relativistic objects, their oscillations must be studied in the framework of General Relativity. The relativistic theory of oscillations was developed in a series of papers by Thorne and coauthors (Thorne & Campolattaro 1967; Price & Thorne 1969; Thorne 1969a,b; Campolattaro & Thorne 1970; Ipser & Thorne 1973). In particular, the rapid (~ 1 s) damping of p-modes with multipolarity $l = 2$ by gravitational radiation was demonstrated by Thorne (1969a). An exact treatment of general-relativistic effects is complicated, but in many cases it is possible to use the relativistic Cowling approximation (McDermott et al. 1983). An analysis of various oscillation modes and mechanisms for their dissipation was carried out by McDermott (1988). Let us also note the review paper by Stergioulas (2003), which contains an extensive bibliography. As a rule, one considers neutron star oscillations with low values of l .

Although neutron stars are objects at the final stage of

stellar evolution, they can be seismically active for many reasons. Possible mechanisms for the generation of oscillations have been widely discussed in the literature (see, e.g., McDermott (1988); Stergioulas (2003) and references therein). Recently, much attention has been paid to r-modes – vortex oscillations that can be generated in rapidly rotating neutron stars and accompanied by powerful gravitational radiation. In addition, oscillations can be excited in neutron stars, for example, during X-ray bursts (nuclear explosions in outermost layers of accreting neutron stars), bursting activity of magnetars (anomalous X-ray pulsars and soft gamma-ray repeaters; see, e.g., Kaspi (2004)), and glitches (sudden changes of spin periods) of ordinary pulsars.

In this paper we focus on high-frequency (~ 100 kHz) pressure oscillations (p-modes) with high multipolarity $l \gtrsim 100$ localized in neutron star envelopes (crusts). In our previous paper (Chugunov & Yakovlev 2005) we have studied these oscillations for $l \gtrsim 500$. In that case p-modes are localized in the outer envelope (before the neutron drip point, at densities $\rho \lesssim 4 \times 10^{11}$ g cm $^{-3}$), where the equation of state (EOS) of stellar matter is relatively smooth. Accordingly, the oscillation spectrum is simple and well established.

In the present paper we extend our analysis to p-modes with lower l . These oscillations penetrate into the inner envelope of the star, where the EOS undergoes considerable softening due to neutronization and becomes more complicated (essentially different for ground-state and accreted matter).

* E-mail: andr.astro@mail.ioffe.ru

We show that the neutron drip affects strongly the oscillation spectrum. If detected, this spectrum would give valuable information on the EOS in neutron star envelopes and also on global parameters of neutron stars (their masses and radii).

2 FORMALIZM

Following Chugunov & Yakovlev (2005) we study oscillations localized in a thin neutron star envelope. It is convenient to use the approximation of a plane-parallel layer, and write space-time metric in the envelope as

$$ds^2 = c^2 dt^2 - dz^2 - R^2 (d\vartheta^2 + \sin^2 \vartheta d\varphi^2), \quad (1)$$

where the local time t and local depth z are related to the Schwarzschild time \tilde{t} and circumferential radius r by

$$t = \tilde{t} \sqrt{1 - R_G/R}, \quad z = (R - r)/\sqrt{1 - R_G/R}, \quad (2)$$

$r = R$ is the circumferential radius of the stellar surface, ϑ and φ are spherical angles, $R_G = 2GM/c^2$ is the gravitation radius, and M is the gravitational mass of the neutron star. The metric (1) is locally flat and allows us to use the Newtonian hydrodynamic equations for a thin envelope with the gravitational acceleration

$$g = \frac{GM}{R^2 \sqrt{1 - R_G/R}}. \quad (3)$$

The pressure in the envelope is primarily determined by degenerate electrons and neutrons (in the inner envelope), being almost independent of temperature T . Accordingly, we can use the same zero-temperature EOS for the equilibrium structure of the envelope and for perturbations. Employing this EOS, we neglect the buoyancy forces and study p-modes. The linearized hydrodynamic equations (for a non-rotating star) can be rewritten as (see, e.g., the monograph by Lamb 1975)

$$\frac{\partial^2 \phi}{\partial t^2} = c_s^2 \Delta \phi + \mathbf{g} \cdot \nabla \phi, \quad (4)$$

where ϕ is the velocity potential and $c_s^2 \equiv \partial P_0 / \partial \rho_0$ is the squared sound speed. The velocity potential can be presented in the form

$$\phi = e^{i\omega t} Y_{lm}(\vartheta, \varphi) F(z), \quad (5)$$

where ω is an oscillation frequency, and $Y_{lm}(\vartheta, \varphi)$ is a spherical function (see, e.g., Varshalovich et al. (1988)). An unknown function $F(z)$ obeys the equation

$$\frac{d^2 F}{dz^2} + \frac{g}{c_s^2} \frac{dF}{dz} + \left(\frac{\omega^2}{c_s^2} - \frac{l(l+1)}{R^2} \right) F = 0. \quad (6)$$

The boundary condition at the stellar surface is $F(0) = 0$. It comes from the requirement of vanishing Lagrange variation of the pressure at the surface. The formal condition $\lim_{z \rightarrow \infty} F(z) = 0$ in the stellar interior should be imposed to localize oscillations in the envelope. Of course, the actual variable z is finite and the real depth of oscillation localization will be controlled in calculations. The EOS of matter in neutron star envelopes contains a sequence of first-order phase transitions associated with changes of nuclides with growing density. These phase transitions are relatively weak (the density jumps do not exceed 20 per cent). We should

add boundary conditions at all phase transitions within the envelope. These are two well known conditions at a plain boundary of two liquids (Lamb 1975). The first condition can be written as

$$F_1'(z) = F_2'(z). \quad (7)$$

It ensures equal radial velocities at both sides of the boundary. The second condition is

$$F_1 = \frac{\rho_2}{\rho_1} F_2 + \left(\frac{\rho_2}{\rho_1} - 1 \right) \frac{g}{\omega^2} F_1'. \quad (8)$$

It comes from the requirement of pressure continuity at the boundary. Note, that the boundary conditions (7) and (8) provide a source of buoyancy which leads to the density discontinuity of g-modes (see, e.g., McDermott 1990).

Oscillations of a plane-parallel layer for a polytropic EOS ($P \propto \rho^{1+1/n}$, n being the polytropic index) were studied analytically by Gough (1991). In this case, the squared sound speed is $c_s^2 = g z/n$. The solution for eigenfrequencies is

$$\omega_k^2 = \frac{g}{R} \sqrt{l(l+1)} \left(\frac{2k}{n} + 1 \right), \quad (9)$$

and eigenmodes are given by

$$F_k(z) = \exp\left(-\sqrt{l(l+1)} \frac{z}{R}\right) L_k^{(n-1)}\left(2\sqrt{l(l+1)} \frac{z}{R}\right), \quad (10)$$

where $L_k^{(n-1)}(x)$ is a generalized Laguerre polynomial (Abramovitz & Stegun 1971), and $k = 0, 1, \dots$ is the number of radial nodes.

Note, that the mode with $k = 0$ does not have any radial nodes; its properties are independent of the polytropic index n . This mode corresponds to the vanishing Lagrangian variation of the density (incompressible motion). Adding the condition $\Delta \phi = \Delta \mathbf{U} = 0$ to Eq. (4), one can easily show that the mode with the frequency

$$\omega_0^2 = \frac{g}{R} \sqrt{l(l+1)} \quad (11)$$

and the eigenfunction $F_0(z)$, defined by Eq. (10), is the proper mode for a wide class of EOSs. Note, that the boundary conditions (7) and (8) are automatically satisfied for this mode, and it is continuous at phase transitions. The oscillation frequency redshifted for a distant observer is

$$\begin{aligned} \tilde{\omega}_0^2 &= \left(1 - \frac{R_g}{R}\right) \frac{g}{R} \sqrt{l(l+1)} \\ &= \frac{GM}{R^3} \sqrt{1 - R_G/R} \sqrt{l(l+1)}. \end{aligned} \quad (12)$$

The frequency ω_0 will be used to normalize eigenfrequencies of other p-modes. The number of radial nodes k will be used to enumerate the modes.

2.1 Self-similarity and scaling

Let us use the equation of hydrostatic equilibrium $dP/dz = \rho g$ and transform Eq. (6) taking the equilibrium pressure P as an independent variable,

$$\frac{d^2 F}{dP^2} + \frac{2}{\rho c_s^2} \frac{dF}{dP} + \frac{1}{\rho^2} \left(\frac{\omega^2}{g^2 c_s^2} - \frac{l(l+1)}{g^2 R^2} \right) F = 0. \quad (13)$$

The boundary conditions (7) and (8) can be written as

$$\rho_1 \frac{dF_1}{dP} = \rho_2 \frac{dF_2}{dP}, \quad (14)$$

$$F_1 = \frac{\rho_2}{\rho_1} F_2 + \left(\frac{\rho_2}{\rho_1} - 1 \right) \frac{g^2}{\omega^2 \rho_1} \frac{dF_1}{dP}. \quad (15)$$

Therefore, Eq. (13) with the boundary conditions (14), (15) and with regularity requirement can be treated as the equation for an eigennumber $\lambda = \omega^2/g^2$ containing the scaling parameter $\zeta = \sqrt{l(l+1)}/(gR)$ (with $\zeta \approx l/(gR)$ for $l \gg 1$). Accordingly, the eigenfrequencies can be written as

$$\omega_k^2 = g^2 g_k(\zeta) = \omega_0^2 f_k(\zeta). \quad (16)$$

Here, $g_k(\zeta)$ and $f_k(\zeta)$ are functions which can be calculated numerically. They are universal for all neutron stars with a given EOS in the envelope. The velocity potentials F_k are also universal functions of P . Therefore, p-mode oscillations in stellar envelopes are self-similar and can be easily rescaled to a neutron star with any radius and mass. In principle, this can be used to determine R and M (see Sec. 3.2).

3 NUMERICAL RESULTS

Numerical results are presented for a “canonical” neutron star model, with the mass $M_c = 1.4M_\odot$ and the radius $R_c = 10$ km. For this model, we have $g_c \approx 2.42 \times 10^{14}$ cm s⁻²,

$$\omega_0 \approx 1.56 \times 10^5 [l(l+1)/10^4]^{1/4} \text{ s}^{-1} \quad (17)$$

and (for a distant observer)

$$\tilde{\omega}_0 = \omega_0 \sqrt{1 - R_G/R} \approx 1.19 \times 10^5 [l(l+1)/10^4]^{1/4} \text{ s}^{-1}. \quad (18)$$

Oscillation frequencies have been determined via a series of iterative trials, checking the coincidence of the mode number and the number of radial nodes.

3.1 Equations of state

We employ two models of matter in neutron star envelopes, the accreted and ground-state matter. For the accreted matter, we use the EOS of Haensel & Zdunik (1990) (HZ). It was derived by following transformations of atomic nuclei (beta captures, emission and absorption of neutrons, pycnonuclear reactions) in an accreted matter element with increasing the pressure. The EOS was calculated for the densities from $\rho = 3.207 \times 10^7$ g cm⁻³ to 1.462×10^{13} g cm⁻³. For lower densities, we have taken the matter composed of ⁵⁶Fe and the EOS of degenerate electrons with electrostatic corrections. For higher densities, we use the EOS of the ground-state matter presented by Baym, Pethick & Sutherland (1971) (BPS) because, as remarked by Haensel & Zdunik (1990), the HZ EOS becomes very similar to the BPS EOS at $\rho > 10^{13}$ g cm⁻³.

We have also considered envelopes composed of the ground-state (cold catalyzed) matter. In the outer envelope we use the EOS of Haensel & Pichon (1994) (HP) and the recent EOS of Rüstler, Hempel & Schaffner-Bielich (2005) (RHS). For the inner envelope, we employ the EOS of Negele & Vautherin (1973).

Phase transitions in these EOSs have been treated carefully using the boundary conditions (7) and (8) at any phase

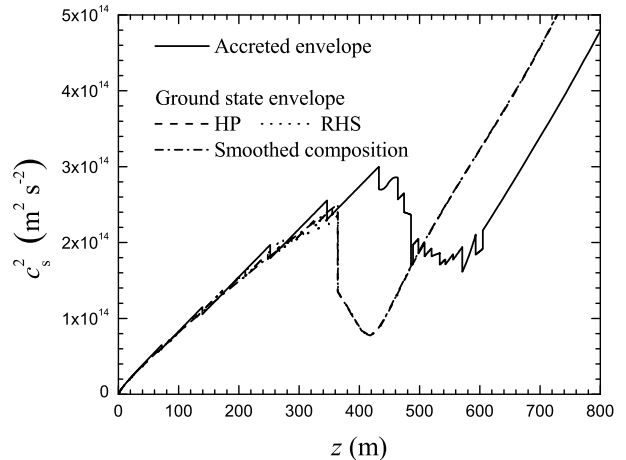


Figure 1. The squared sound speed c_s^2 as a function of depth z . Solid line is for an accreted envelope. The dashed, dotted and dash-and-dotted lines are for the HP, RHS and SCM EOSs of the ground-state matter.

transition. For comparison, we have also employed the model of the outer envelope composed of ground-state matter with a smoothed composition (the smooth composition model – SCM). In the latter case we have included only a large density jump at the neutron drip boundary between the inner and outer envelopes.

The squared sound speed c_s^2 as a function of depth z for all these EOSs is shown in Fig. 1. The solid line is for the accreted envelope; the dashed, dotted and dash-and-dot lines are for the HP, RHS and SCM EOSs of the ground-state matter. The different versions of the ground-state EOS show approximately the same sound speed profiles, but the profile in the accreted envelope is significantly different.

The depth of the accreted envelope (up to the density 2.004×10^{14} g cm⁻³, which is the largest density in the envelope, where the atomic nuclei are present, for the BPS EOS) is $z \approx 1150$ m. For all models of the ground-state matter, the largest density in the envelope has been taken $\approx 1.7 \times 10^{14}$ g cm⁻³; the envelope depth is $z \approx 985$ m.

3.2 Eigenfrequencies

Figures 2 and 3 show squares of dimensionless eigenfrequencies ω_k^2/ω_0^2 versus multipolarity l for accreted and ground-state envelopes of the canonical neutron star. Because of the scaling (16) the figures can be easily transformed to a star with any gravity g and radius R by changing scale of the l axis by a factor of $gR/(g_c R_c)$.

For any envelope, the modes with $l \gtrsim 300$ can be subdivided into two groups, with a pronounced linear dependence and with a weak dependence of ω_k^2/ω_0^2 on l . As will be shown in Section 3.4, the modes of the first type (*the inner modes*, shown by thicker lines in Fig. 2) are localized in the vicinity of the neutron drip point, while the modes of the second type (*the outer modes*) are localized in the outer envelope. In Figs. 2 and 3 one can see a number of quasi-intersections. When passing through a quasi-intersection point (with growing l), an inner mode gains an additional radial node, but an outer mode loses one.

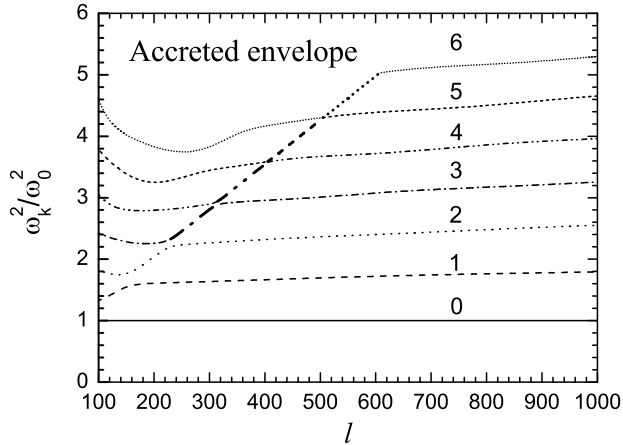


Figure 2. Squared normalized eigenfrequencies ω_k^2/ω_0^2 versus multipolarity l for the accreted envelope of the canonical neutron star. The numbers next to curves indicate the number of radial nodes. Thin parts of the curves correspond to the outer modes and (for low l) modes which spread over the entire envelope, while thick segments refer to the inner modes.

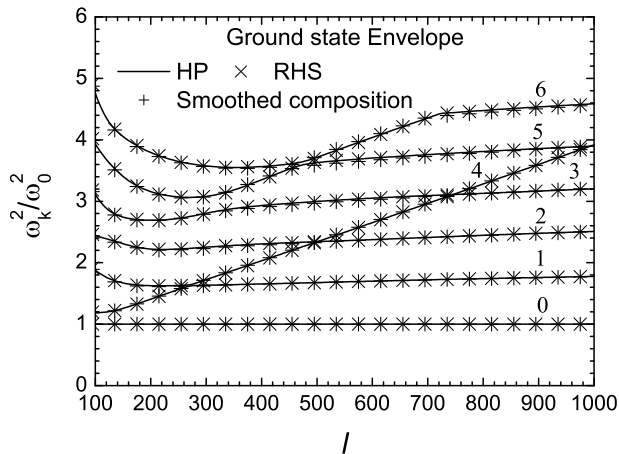


Figure 3. Same as in Fig. 2, but for the envelope composed of the ground-state matter (the inner modes are not emphasized). Lines are for the HP EOS; crosses ‘x’ are for the RHS EOS; crosses ‘+’ are for the SCM.

Let us consider the outer modes. The eigenfrequencies are the same (within $\sim 1\%$) for all ground-state EOSs (see Fig. 3). For the accreted envelope, eigenfrequencies are larger because the EOS is stiffer. With decreasing l , oscillations penetrate deeper into the outer envelope, where the EOS is softer because electrons become relativistic, and because they undergo beta-captures. It leads to a gradual decrease of ω_k^2/ω_0^2 . As in the model with the polytropic EOS, given by Eq. (9), separations between squares of neighboring dimensionless eigenfrequencies ω_k^2/ω_0^2 are approximately constant for a fixed l . The weak decrease of separations with the growth of k is due to the penetration of oscillations into deeper layers of the star, where the EOS is softer. The latter effect is more pronounced for the ground-state matter owing to a stronger softening of the EOS. Finally, at $l \sim 1000$ the outer p-modes are localized in the outer layers of the

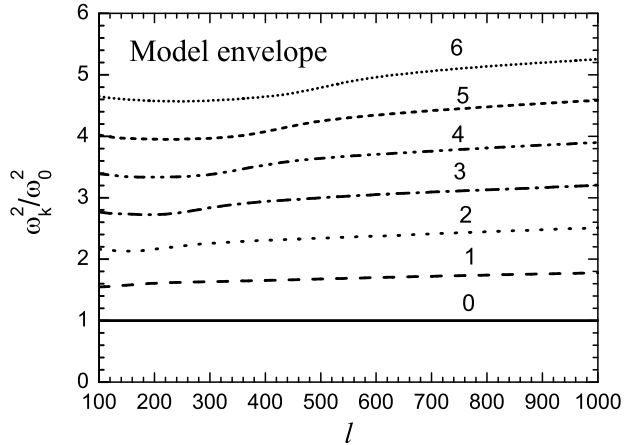


Figure 4. Same as in Fig. 2, but for a model envelope in which the outer envelope is composed of the ground-state matter and the inner envelope is composed of ^{116}Se .

outer envelope, where the matter is composed of ^{56}Fe nuclei for both accreted and ground-state EOSs. Accordingly, eigenfrequencies become nearly equal.

Naturally, the oscillation frequencies of outer modes with $l \gtrsim 500$ for the ground state envelope are the same as calculated by Chugunov & Yakovlev (2005).

To demonstrate explicitly that inner modes are caused by the neutron drip in the inner envelope, in Fig. 4 we present eigenfrequencies for a model envelope without any neutron drip. Here we employ the RHS EOS in the outer envelope but assume that the inner envelope is composed of ^{116}Se ions (the last element at the outer envelope) and electron gas (no free neutrons). The oscillation spectrum does not contain any inner modes. A small decrease of ω_k^2/ω_0^2 for $200 \lesssim l \lesssim 500$ is produced by the softening of the EOS at the bottom of the outer envelope. The growth of frequencies at $l \sim 100$ is caused by the penetration of oscillations into the inner envelope, where our model EOS is polytropic (with the index $n = 3$). Accordingly, oscillation frequencies tend to the values provided by the polytropic model (9).

3.3 Inferring M , R , and the crustal EOS from oscillation spectrum

If detected, outer modes would give us $\tilde{\omega}_0$, and therefore $MR^{-3}\sqrt{1-R_G/R}$; see Eq. (12). A detection of the only one fundamental mode ($k = 0$) would be sufficient to determine $MR^{-3}\sqrt{1-R_G/R}$. A detection of several outer modes (with different l and/or k) would confirm and strengthen this determination.

Our calculations show that for the inner modes the ratio $\omega_{\text{in}}^2/\omega_0^2$ is a linear function of l . Using the scaling relation (16) we can present this linear dependence in the form

$$\omega_{\text{in}}^2/\omega_0^2 = A + Bl, \quad B = \beta/(g_{14}R_6). \quad (19)$$

Here, g_{14} is the surface gravity in units $10^{14} \text{ cm s}^{-2}$, $R_6 = R/10^6 \text{ cm} = R/10 \text{ km}$, while A and β are dimensionless constants determined by the EOS in a neutron star envelope.

For the canonical neutron star with the ground-state envelope, we obtain $A = 0.75$ and $B = 0.0032$ in the case of

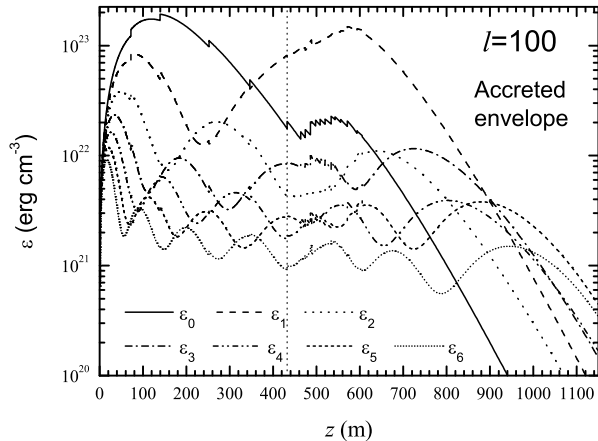


Figure 5. Angle-averaged energy density of oscillations for modes with $l = 100$ in the accreted envelope. The subscript of ε indicates the number of radial nodes. The root-mean-square amplitude of radial displacements at the stellar surface is 1 m. The vertical dotted line shows the boundary between the inner and outer envelopes.

inner modes with lowest frequencies. For the same star with the accreted crust we have $A = 0.65$ and $B = 0.0073$. The values of B allow us to determine β . In this way we obtain

$$A = 0.75, \quad \beta = 0.0013 \quad \text{for ground state crust;} \quad (20)$$

$$A = 0.65, \quad \beta = 0.0030 \quad \text{for accreted crust.} \quad (21)$$

Hence, the difference between the ground-state and accretion envelopes is quite pronounced in oscillation spectra.

Therefore, if several (minimum two) inner modes could be detected in addition to outer modes, their frequencies could be fitted by a function (19) and the values of A and B could be determined. An accurate determination of A would enable one to distinguish between the ground-state and accretion envelopes. The value of B would give then gR . Combining this gR with the value $gR^{-1} \sqrt{1 - R_G/R}$, determined from the detection of the outer modes, one would get a simple system of two equations for two unknowns, M and R . Thus, a detection of one outer mode and several inner ones could in principle enable one to discriminate between the ground-state and accreted envelopes and determine neutron star mass and radius.

3.4 Eigenmodes

Figures 5–8 show profiles of the angle-averaged energy density of oscillations as a function of z . The root-mean-square amplitude of radial displacements of the stellar surface has been set equal to 1 m. The subscript of ε indicates the number of radial nodes. The vertical dotted line marks the boundary between the inner and outer envelopes ($z \approx 432$ m for the accreted envelope, and $z \approx 364$ m for all ground-state envelopes of the canonical neutron star).

Figure 5 depicts eigenmodes with $l = 100$ for the accreted envelope. The modes are spread over the entire envelope; their subdivision into the outer and inner modes is not obvious. However, some traces of two mode types are visible. The mode with one radial node (the dashed line), whose

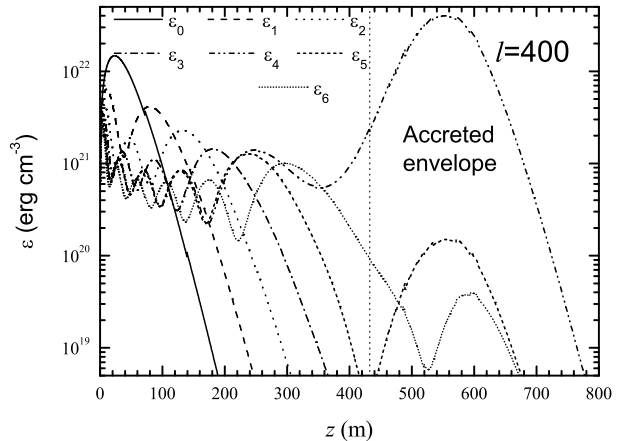


Figure 6. Same as in Fig. 5 for modes with $l = 400$ in the accreted envelope.

frequency belongs to the branch of the outer modes, is primarily localized in the vicinity of the neutron drip point. However, other modes do not demonstrate this feature. The effects of phase transitions are relatively small ($\sim 20\%$) and only slightly noticeable in Figure 5. They are local and do not change global (on scales of $\gtrsim 20$ m) energy density profiles.

Figure 6 shows eigenmodes with $l = 400$ for the accreted envelope. This value of l is very close to the quasi-intersection point for the modes with 4 and 5 radial nodes (see Fig. 2). The subdivision into the outer and inner modes is clear – the modes with $k = 0, 1, 2, 3, 5, 6$ radial nodes are localized in the outer envelope, but the energy of the mode with $k = 4$ is concentrated in the outer part of the inner envelope. This subdivision is the same as in Section 3.2 (see Figure 2). The energy-density profiles of the fourth and fifth modes are very similar at $z \lesssim 250$ m, but at $z \sim 500$ m the energy densities differ by more than two orders of magnitude! The outer modes ‘feel’ the lowering of the sound speed in the outer layers of the inner envelope (see Fig. 1) and increase their energy density in this region. However, the increase is not so large as for the inner modes. The signatures of phase transitions are very small ($\sim 10\%$) and hardly visible in Figure 6. They are local and do not change energy density profiles on scales $\gtrsim 20$ m.

Figures 7 and 8 are plotted for the ground-state envelope with the RHS EOS. The results for the HP and SCM are qualitatively the same.

Figure 7 depicts eigenmodes with $l = 100$. The modes are localized in the entire envelope and cannot be subdivided into the outer and inner ones. The traces of these two types of modes are weaker than for the accreted envelope (see Fig. 5). The signatures of phase transitions in the outer envelope are small $\lesssim 10\%$ and have scales ~ 10 m. They are noticeable only for the modes with a few number of radial nodes. Many modes show large ($\sim 50\%$) jumps of the energy density at the neutron drip point.

Figure 8 shows eigenmodes with $l = 500$. This value of l is close to the quasi-intersection point for modes with $k = 2$ and 3 and with $k = 5$ and 6 (see Fig. 3). The modes can obviously be subdivided to the two types. The modes with

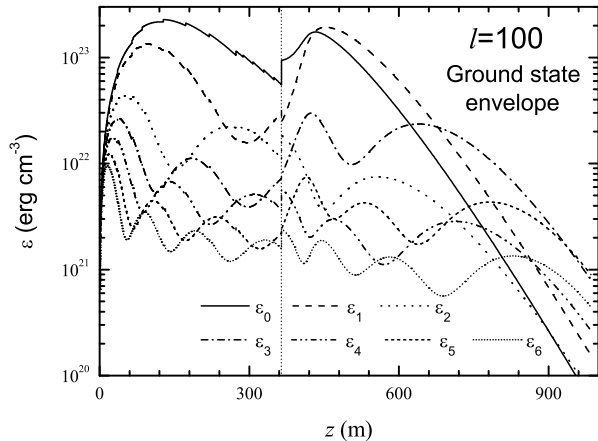


Figure 7. Same as in Fig. 5 for modes with $l = 100$ in the ground-state envelope.

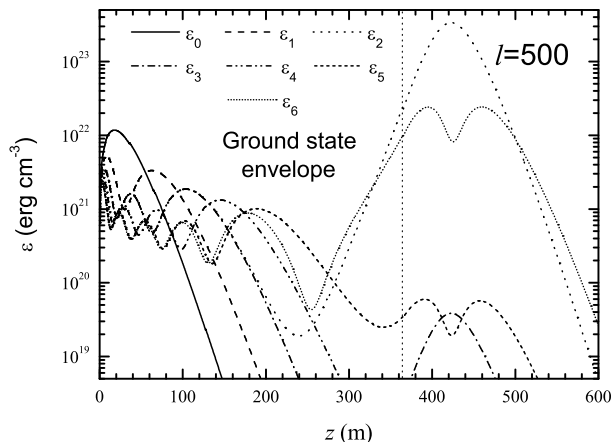


Figure 8. Same as in Fig. 5 for modes with $l = 500$ in the ground-state envelope.

$k = 0, 1, 3, 4, 5$ are localized in the outer envelope; the energy of the modes with $k = 2$ and 6 is concentrated near the neutron drip point. The subdivision of modes is the same as suggested in Section 3.2 on the basis of Figure 3. The energy profiles of the second and third modes are very close for $z \lesssim 200$ m, but for $z \sim 420$ m the energy density differs by more than three orders of magnitude. Qualitatively the same feature is demonstrated by the fifth and sixth modes. The outer modes ‘respond’ to the lowering of the sound speed after the neutron drip point by increasing the energy density in this region. This increase is greater for the second and fifth modes whose frequencies are close to the frequencies of the inner modes. However, it is not so large as for the inner modes. The signatures of phase transitions in the outer envelope are extremely small ($\sim 5\%$) and are almost invisible in Figure 8. The scales of such features are ~ 1 m. The large phase transition at the neutron drip point produces the signature with the same properties.

4 CONCLUSIONS

We have studied high-frequency pressure oscillations which are localized in the envelopes of neutron stars composed of the accreted or ground-state matter.

Our main conclusions are as follows.

(1) The oscillations are almost insensitive to various modifications of the EOS for the ground-state matter (section 3.2). All EOSs we have used (HP, RHS, SCM) give the same oscillation spectrum.

(2) The neutron drip and associated softening of the EOS in the inner envelope do not affect strongly the spectrum of the well known (outer) oscillation modes which are localized predominantly in the outer envelope (section 3.2).

(3) However, the neutron drip leads to the appearance of inner oscillation modes localized mostly near the neutron drip point (section 3). The spectrum of these modes is sensitive to the EOS in the envelope (accreted or ground-state).

(4) The p-mode oscillation problem is self-similar (in the plane-parallel approximation). Once the problem is solved for one stellar model, it can easily be rescaled to neutron star models with any mass and radius (but the same EOS in the envelope; see section 2.1).

(5) A detection and identification of one outer mode and several inner modes would enable one to discriminate between the ground-state and accreted envelope and determine neutron star mass and radius (section 3.3). For example, a detection of the fundamental mode with $l = 900$ at the frequency 74 kHz and of two inner modes with $l = 300$ and $l = 900$ at 56 kHz and 140 kHz, respectively, would indicate a canonical neutron star with the ground-state envelope.

Therefore, high-frequency pressure modes are excellent tools to explore the physics of matter in neutron star envelopes and to determine masses and radii of neutron stars. The oscillation frequencies could be detected by radio-astronomical methods very precisely. A detailed analysis of pulse shapes of some radio pulsars reveals that oscillations with large multipolarity are possibly excited there (Clemens & Rosen 2004) but their frequencies are ~ 30 Hz, so that they are not high-frequency p-modes we discuss here.

A search for high-frequency p-modes could be useful. High-multipolarity p-modes do not damp very quickly because they do not produce any powerful gravitational or electromagnetic emission (see, e.g., Chugunov & Yakovlev 2005). They are robust because they are relatively independent of the thermal state of the star, and they should not be strongly affected by neutron star magnetic fields. The inner p-modes, localized in the inner envelope, could be easily triggered by pulsar glitches, which are thought to occur just in inner envelopes of pulsars. Chugunov & Yakovlev (2005) studied the dissipation of p-modes localized in the outer envelope; this dissipation is mainly produced by the shear viscosity. It may be enhanced by thin viscous layers near numerous nuclear phase transitions. The viscosity in these layers can be diffusive or turbulent. Note, that fundamental modes do not produce viscosity layers because they pass phase transitions without velocity discontinuities (see Sec. 2). Their dissipation is not enhanced by phase transitions.

Finally, p-modes in neutron star envelopes are relatively insensitive to the EOS and composition of neutron star cores. However, these modes can be useful to discriminate between ordinary neutron stars and strange stars with

crust. The latter stars are thought to contain extended cores composed of strange quark matter. Nevertheless, a core is assumed to be surrounded by an envelope of normal matter (see, e.g., Zdunik 2002), so that a strange star with the crust may look like an ordinary neutron star from outside. The density of the normal matter in a strange star does not exceed the neutron drip density. The pressure modes in the envelopes of such stars should easily ‘feel’ underlying dense quark matter, and the oscillation spectrum would reflect the presence of the quark core. We intend to consider this effect in a future publication.

ACKNOWLEDGMENTS

I am grateful to D.G. Yakovlev for discussions. This work was supported by a grant of the “Dynasty” Foundation and the International Center for Fundamental Physics in Moscow, by the Russian Foundation for Basic Research (project no. 05-02-16245), and by the Program of Support for Leading Scientific Schools of Russia (NSh-1115.2003.2).

REFERENCES

- Abramowitz M., Stegun I.A., 1971, Handbook of Mathematical Functions, Dover, New York
- Baym G., Pethick C., Sutherland P., ApJ, 1971, 170, 299
- Campolattaro A., Thorne K.S., 1970 ApJ, 159, 847
- Chugunov A.I., Yakovlev D.G., 2005, Astr. Rep., 49, 724
- Clemens J.C., Rosen R., 2004, ApJ, 609, 340
- Gough D.O., 1991, in Zahn J-P., Zinn-Justin J., eds, Astrophysical fluid dynamics, Elsevier, Amsterdam, p. 399
- Haensel P., Pichon B., A&A, 1994, 283, 313
- Haensel H., Zdunik J.L., 1990, A&A, 229, 117
- Ipser J.R., Thorne K.S., 1973, ApJ, 181, 181
- Kaspi V.M., 2004, in Camilo F., Gaensler B.M., eds, Young Neutron Stars and Their Environments, Astron. Soc. Pac., San Francisco, p. 231
- Lamb H., 1975, Hydrodynamics, Cambridge Univ. Press, London
- Negele J.W., Vautherin D., 1973, Nucl. Phys. A, 207, 298
- McDermott P.N., 1990, MNRAS, 245, 508
- McDermott P.N., Van Horn H.M., Scholl J.F., 1983, ApJ, 268, 837
- McDermott P.N., Van Horn H.M., Hansen C.J., 1988, ApJ, 325, 725
- Price R., Thorne K.S., 1969, ApJ, 155, 163
- Rüster S.B., Hempel M., Schaffner-Bielich J., 2005, preprint (astro-ph/0509325)
- Stergioulas N., 2003, Living Rev. in Relativity, 6, 3
- Thorne K.S., 1969a, ApJ, 158, 1
- Thorne K.S., 1969b, ApJ, 158, 997
- Thorne K.S., Campolattaro A., 1967, ApJ, 49, 591
- Varshalovich D.A., Moskalev A.N., Khersonskii V.K., 1988, Quantum Theory of Angular Momentum, World Scientific, Singapore
- Zdunik J.L., 2002, A&A, 394, 641